AIAA JOURNAL
Vol. 42, No. 12, December 2004

Calculation of Flows Characterized by Extensive Crossflow Separation

Argyris G. Panaras*
15772 Athens, Greece

Flows with extensive crossflow separation appear in many flying vehicles. Traditionally these types of flows are difficult to simulate accurately, especially if the separation is extensive (flow at high incidence or strong swept shock waves impinging on boundary layers). The present author has shown in previous publications that if the three-dimensional structure of these flows is considered for modifying a conventional turbulence model the efficiency of the model is enhanced considerably. This concept has been demonstrated for the case of the supersonic fin/plate interaction, and it is based on the observation that in turbulent flows characterized by extensive crossflow separation a layer of low turbulence exists close to the surface (underneath the core of the separation vortex). This flow feature has been incorporated into the Baldwin–Lomax algebraic turbulence model by the introduction of a new relation for the calculation of the eddy viscosity within the separation domain. In the present paper, the modified turbulence model is extended for application to more complicated shock-wave/turbulent boundary-layer interactions (crossing shocks) and to high-angle-of-attack flows.

I. Introduction

FLOWS with extensive crossflow separation appear in many practical configurations, for example, subsonic/supersonic flows about slender bodies or delta wings at high incidence or in components of supersonic/hypersonic air vehicles when swept shock waves interact with boundary layers. It is well known that when the interacting boundary layer is turbulent the accuracy of numerical simulations of these flows is marginal.

The present author recently[1] studied the effect on turbulence modeling of the structure of the separation vortex, which appears in a strong swept-shock-wave/turbulent-boundary-layer interaction by calculating a well-documented sharp-fin/plate flow.[2] After the validation of the results with appropriate experimental data, he studied the flowfield by means of stream surfaces starting at the inflow plane within the undisturbed boundary layer, which is initially parallel to the plate. Each of these surfaces was represented by a number of streamlines.

Calculation of the spatial evolution of selected stream surfaces revealed that the inner layers of the undisturbed boundary layer, where the eddy viscosity is high, wind around the core of the separation vortex. However, the outer layers, which have low turbulence, rotate over the separation vortex and penetrate into the separation bubble at the reattachment region forming a low-turbulence tongue, which lies along the plate, underneath the vortex (Fig. 1). The intermittency of the fluid that constitutes the tongue is very small, that is, the flow is almost laminar there. At the initial stage of development, the conical separation vortex is completely composed of turbulent fluid, but as it grows linearly downstream the low-turbulence tongue is formed. By studying additional test cases, Panaras found that the increase in the strength of the interaction results in the folding of higher inviscid layers around the vortex. In the other extreme of a weak interaction, no low-turbulence tongue is formed.

The existence of the low-turbulence tongue underneath the conical separation vortex of a strong swept-shock/turbulent-boundary-layer interaction creates a mixed-type separation bubble: turbulent flow in the vicinity of the separation line and almost laminar flow between the reattachment line and the secondary separation vortex. This type of separation is difficult to simulate accurately because presently used turbulence models are based on the physics of two-dimensional flows, where, in a separation bubble, the whole recirculation region is turbulent.

To improve the accuracy of numerical predictions of swept-shock-wave/turbulent-boundary-layer interactions, Panaras[3] considered the aforementioned physical feature in the derivation of a new equation for the calculation of the eddy-viscosity coefficient in the region of the separation vortex. Panaras followed the Baldwin–Lomax formulation because it is easily implemented in a Navier–Stokes scheme. The model was used for the computation of some of the test cases compiled by Settles and Dodson.[2] The agreement with the experimental data was very good. In addition, the results were given to Knight and Degrez,[4] who compared them with similar calculations contributed by other researchers employing different turbulence models, in order to assess the capability of numerical simulations of three-dimensional shock-wave/turbulent-boundary-layer interactions. The turbulence model proposed by the present author was the only one that predicted the secondary separation in some of the compared flows. An example is shown in Fig. 2 for the Mach = 4, 16-deg-fin case.

In principle, the eddy-viscosity equation developed by Panaras[3] is appropriate for applications to other three-dimensional flows characterized by the appearance of extensive crossflow separation (generation of crossflow vortices). However, this applicability has not been assessed. This is in the focus of the present work. In addition, the analysis is extended to strong crossing-shock-waves/turbulent-boundary-layer interactions, which are established in the supersonic/hypersonic flow between two fins attached on a plate.

II. Modified Algebraic Turbulence Model

A. Single-Fin/Plate Flows

The base of the turbulence model that was developed in Ref. 3 for application to single-fin/plate flows is the original Baldwin and Lomax[5] two-layer algebraic turbulence model. In the inner layer, the eddy viscosity is calculated from the Prandlt–van Driest formulation

$$(\mu_t)_{\text{inner}} = \rho(\kappa D\eta)^2\omega \tag{1}$$

where κ is the von Kármán constant (equal to 0.41), D is the van Driest damping factor, ω is the absolute value of the vorticity, and η is the distance normal to the wall.

Received 8 April 2002; accepted for publication 13 July 2004.

*Consulting Engineer, Agias Elenis 63; anar@central.ntua.gr. Associate Fellow AIAA.

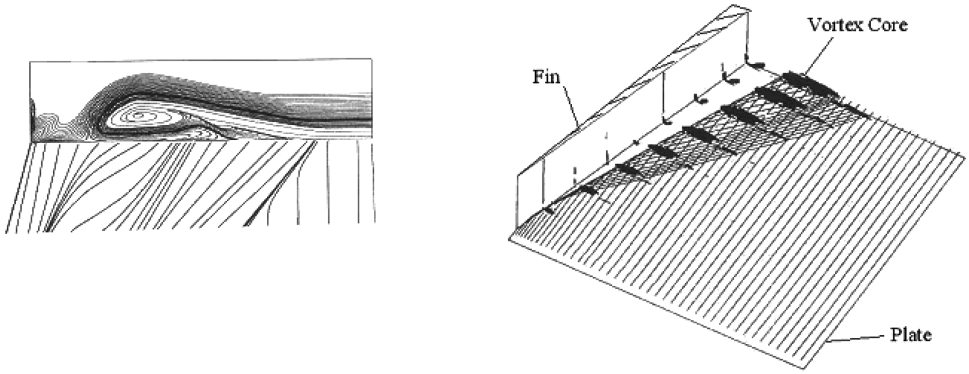

Fig. 1 Structure of the separated flow in a swept-shock/turbulent-boundary-layer interaction.

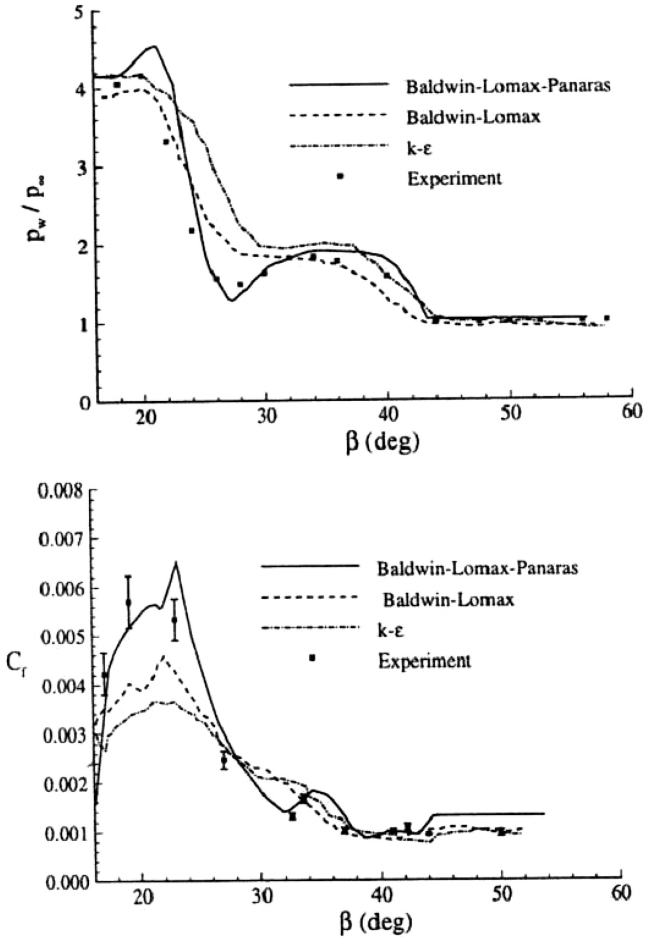

Fig. 2 Application of various turbulence models for the calculation of sharp-fin/plate supersonic flows[4] ($M = 4.0$, $\alpha = 16$ deg).

In the outer layer, the eddy viscosity is calculated from

$$(\mu_t)_{\text{outer}} = C_{\text{cp}}(0.0168\rho F_{\text{wake}}\gamma)$$

$$F_{\text{wake}} = \min\left(\eta_{\max} F_{\max},\, c_{\text{wk}}\eta_{\max} u_{\text{dif}}^2 \big/ F_{\max}\right) \tag{2}$$

The quantity $F_{\max}$ is the maximum value of the moment of vorticity $F(\eta) = \eta\omega D$, and $\eta_{\max}$ is the value of η at which the maximum occurs. The Klebanoff intermittency factor is

$$\gamma = [1 + 5.5(\eta/\delta)^6]^{-1} \tag{3}$$

The quantity u_{dif} is the difference between maximum and minimum velocity in the velocity profile. The thickness of the boundary layer is defined by $\delta = \eta_{\max}/C_{\text{kleb}}$. The constants appearing in the preceding relations are $C_{\text{cp}} = 1.6$, $C_{\text{wk}} = 0.25$, and $C_{\text{Kleb}} = 0.3$.

The calculation procedure introduced by Baldwin and Lomax[5] is very simple. At each surface grid position, an outward search is performed along the corresponding normal gridline for the maximum value of the moment $F_{\max}$ and the distance from the surface $\eta_{\max}$, where it occurs. Then the thickness of the boundary layer at this station is equal to $\delta = \eta_{\max}/C_{\text{Kleb}}$. The calculation of μ_t from Eqs. (1) and (2) along the normal gridline is the final step. At each position, both equations are used for the calculation of μ_t, then their minimum is selected as the appropriate value. However, the simplicity of the calculation procedure is offset, to some extent, by the accuracy of the prediction. Only moderate agreement of the model with experimental data has been reported when applied to separated flows.

For a strong swept-shock/boundary-layer interaction, where the separation has the form of a flat quasi-conical vortex underlaid by a surface layer of almost laminar flow, Panaras[3] proposed the following alternative formulation:

$$F_{\text{wake}} = \eta_{\max} F_{\max} \qquad \text{if} \qquad \eta_{\max} < 1.03\eta_{\text{ref}} \tag{4a}$$

$$F_{\text{wake}} = \frac{\alpha(\eta_{\text{ref}} F_{\text{ref}})^2}{\eta_{\max} F_{\max}} \qquad \text{if} \qquad \eta_{\max} > 1.03\eta_{\text{ref}} \tag{4b}$$

The selection of inverse variation of the new wake function [Eq. (4b)] on the quantity $\eta_{\max} F_{\max}$ guarantees small values of the wake function in the region of the core of the separation vortex because $\eta_{\max}$ and $F_{\max}$ take their largest values there. The small values of the wake function in the region of the vortex core are required because, underneath of the vortex core, the flow is almost laminar. The symbol F_{ref} denotes the maximum value of the moment at a reference point, and η_{ref} is the distance from the surface where it occurs. This point is selected upstream of the separation point in the attached part of the flow. For the particular case of the fin/plate configuration, this selection is trivial because, in any crossflow section, the product $\eta_{\max} F_{\max}$ remains unchanged before the vicinity of the separation point. So it is sufficient to select the reference point away from the separation point, close to the opposite to the fin boundary of the calculation domain.

In the fin/plate configuration where there are two intersecting surfaces, a "modified distance" was proposed by Hung and MacCormack[6] to account for the turbulent mixing length near the intersection of the surfaces:

$$\eta = \frac{2yz}{y + z + \sqrt{(y^2 + z^2)}} \tag{5}$$

where y denotes the distance normal to the plate and z the distance normal to the fin.

Assuming that the applied computation scheme marches in the streamwise x direction and evaluates the flow parameters at each crossflow section, the calculation of the eddy-viscosity model is as

follows. At each cross section the reference point is selected. Equation (4a) gives the wake function in the attached part of the flow, and Eq. (4b) is used within the separated domain. Substitution of the calculated value of the wake function into Eq. (2) provides the eddy viscosity. Experience has shown that the solution converges faster and to the correct solution when the standard Baldwin–Lomax turbulence model is initially applied and the resulting solution, which is not very representative of the real flow, is used as a starting solution for the modified turbulence model.

B. Extension to High-Angle-of-Attack Flows

In high-angle-of-attack flows about slender bodies, fluid flowing circumferentially from the windward to the leeward side separates along a separation line roughly parallel to the longitudinal axis. The fluid rolls up and forms two primary separation vortices on the leeward side. Similar vortices also appear in the high-incidence flow about a delta wing. It is essential to note that, like in the case of the fin/plate flow, there is entrainment of freestream air by the vortices along the streamwise extent of the flow. Thus, the existence of a thin layer of almost laminar flow underneath the core of the pair of the vortices is expected.

In the case of the high-angle-of-attack flows, the boundary-layer thickness changes considerably along the circumferential direction in any cross section of the flow. Its minimum value is observed on the windward symmetry plane, and it gradually thickens as the separation point is approached. Therefore, in any cross section the parameters $\eta_{\max}$ and $F_{\max}$ vary considerably between the windward symmetry plane and the separation point. Thus the selection of the reference point required for the evaluation of Eq. (4b) is not trivial as in the case of the fin/plate configuration. For the purposes of the present study, the reference point was selected close to the separation point in the attached part of the flow. Assuming that the circumferential direction is denoted by the index J, the reference point was defined as $J_{\text{ref}} = J_{\text{sep}} - 4$, that is, four computational points ahead of the separation point at each cross section. The margin of four points ahead of the separation point was considered as necessary because, as the separation point is approached, a significant increase of the value of the parameters $\eta_{\max}$ and $F_{\max}$ is observed.

For the practical application of this approach, at each cross section of the flow the separation point J_{sep} is found by numerically surveying the direction of the circumferential velocity component of the first grid point off the surface. Because the velocity component can change directions several times in the separated region, the search starts from the windward symmetry plane where the flow is attached and proceeds towards the leeward symmetry plane. The separation point for each cross section is where the first circumferential velocity component sign change occurs.

A parametric analysis of the constant α of Eq. (4b), covering the range $\alpha = 2.0$–5.0, has been applied to the ogive-cylinder flow (described in Sec. III.B). The parametric analysis indicated that there is some dependence of the results on the value of the parameter α. But this dependence is not significant, and so the value $\alpha = 3.0$ was assumed for the high-angle-of-attack test cases.

C. Crossing Shock Interactions

A crossing-shock-wave/turbulent-boundary-layer interaction develops on a configuration consisting of two fins, or wedges, attached normal to a flat plate. The resulting flow is very complicated, even if the fins are symmetric. Knight[7] examines the computational aspects of the crossing-shock interactions. The flow consists of the two counter-rotating quasi-conical vortices, which are generated by the individual single fins, and the intersecting shock waves. The initial flat conical vortices interact and gradually become oriented vertically in a mushroom-shaped separation region, which occupies a major portion of the exit area of the dual-fin geometry. Also, the two shocks interact mutually and reflect on the fins forming a very complicated flowfield. Therefore, the crossing-shock configuration is a severe test for a turbulence model. Because the pair of the separation vortices, before their confluence, follows the physics on which the present model is based, the present model was applied in Ref. 3 to a symmetric crossing-shock test case ($M = 3.9$, 15 deg $\times$ 15 deg) compiled by Settles and Dodson.[2]

The calculation procedure described in Sec. II.A for the single-fin cases was used in the crossing-shocks test case. The only difference was the application of a symmetry condition along the centerline of the plane. The results were included in the comparison of calculations by an international group of researchers prepared by Knight and Degrez.[4] According to the authors, the Baldwin–Lomax–Panaras model provided the best prediction of surface pressure, although it underestimated the peak pressure by 16%. All of the computations displayed generally poor agreement for the skin friction. The Baldwin–Lomax–Panaras model displayed the smallest error.

In the course of the present study, the application of Eq. (4) to a stronger symmetric crossing-shock interaction ($M = 5.0$, 23×23 deg) gave very bad results in the interaction region of the two flat vortices, which are generated by the individual fins. The surface flow imprint of the interacting vortices was spread much more in the spanwise direction than in the experiments, whereas the surface pressure along cross sections within the same region had very low values compared to the experimental evidence. This behavior indicated that the actual flow is more turbulent than that predicted by the present model.

The preceding observation led to the decision to use the following alternative relation instead of Eq. (4b), in which the wake function, and correspondingly the eddy viscosity, takes a greater value than that given by Eq. (4b) for the same value of the product $\eta_{\max} F_{\max}$:

$$F_{\text{wake}} = \frac{\alpha (\eta_{\text{ref}} F_{\text{ref}})^{\frac{3}{2}}}{\sqrt{\eta_{\max} F_{\max}}} \tag{6}$$

It will be shown in the next section that this formula considerably improved the results.

III. Results

A. Crossing-Shock Interactions

1. *Experiments and Numerical Method*

Results for very strong crossing-shock-wave/turbulent-boundary-layer interactions will be presented in this section. The experiments were studied by Schuelein and Zheltovodov[8] at the German Aerospace Center (DLR) in the supersonic/hypersonic Ludwieg-Tube (RWG) at $M_\infty = 5$. Two symmetric double-fin configurations were examined: one with fin angle $\beta = 18$ deg and the other with 23 deg. The stagnation conditions were $P_0 = 2.2$ MPa and $T_0 = 427$ K, resulting in a freestream unit Reynolds number of 36.5×10^6/m. The incoming boundary layer was an equilibrium turbulent boundary layer with an isothermal wall ($T_w = 295$ K).

The boundary and momentum thicknesses were $\delta_0 = 3.8$ mm and $\theta = 0.157$ mm at a distance of $6\delta_0$ upstream of the fin leading edge. The measurements consisted of surface flow visualization by an oil film technique and pressure measurements along the centerline and at some cross sections of the flow.

The configurations are shown in Figs. 3 and 4. It can be seen in these figures that the flat plate terminates before the fins terminate. This condition is difficult to simulate numerically, but its effect can be assumed to be secondary. More important in our opinion is the fact that at the trailing edge of the plate there is confluence of the high-pressure air that passes through the fins and the freestream air that flows along the lower surface of the plate. This mixing can have an upstream influence on the flow inside the fins. This effect is not possible to simulate accurately. The standard practice[9] is to model the trailing region as an expansion by inserting a downward ramp. We applied this technique to the 23×23 deg test case, using a ramp of angle 40 or 60 deg. The results indicated that the upstream effect on the wall pressure along the centerline was very small compared to the experimental evidence. For this reason, in the present calculations we terminate the calculation domain at the end of the plate assuming zero gradients of the flow parameters. This assumption corresponds to continuation of the converging passage, that is, increasing pressure. Thus, close to the outflow plane the computed flow is not expected to coincide with the experimental one. This

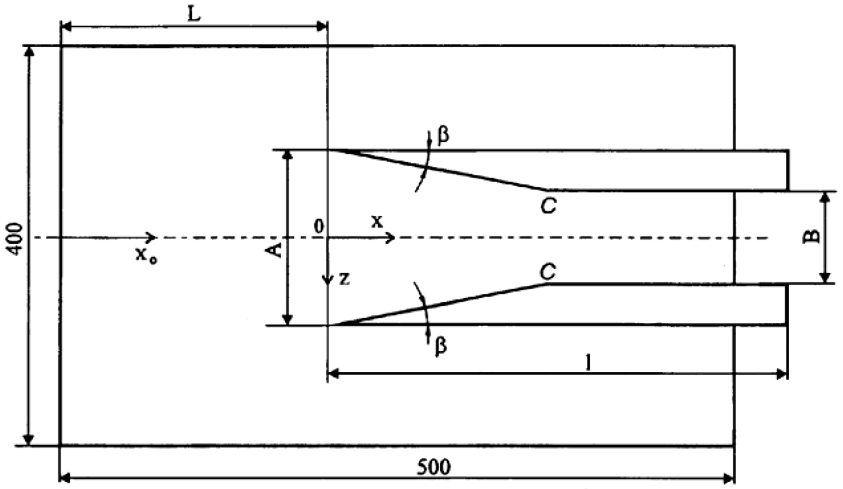

a Short Fins (SF, β = 8°, 12°, 18°)

Fig. 3 Crossing-shocks configuration: 18 × 18 deg.

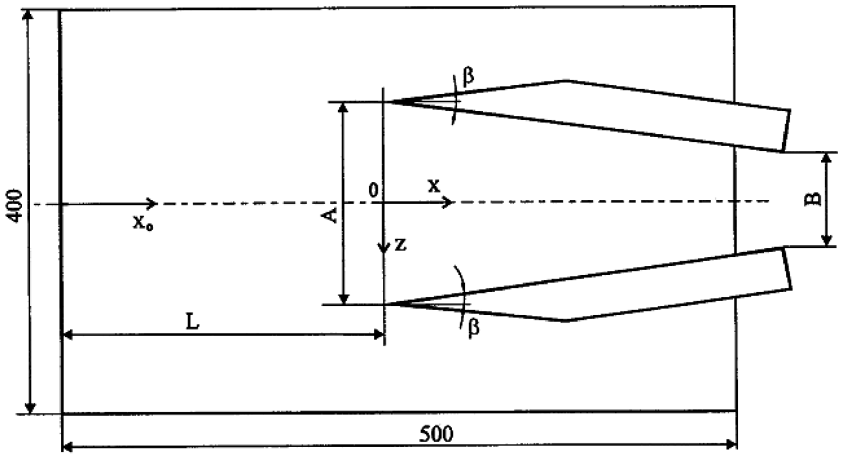

b Long Fins (LF, β = 23°)

Fig. 4 Crossing-shocks configuration: 23 × 23 deg.

condition is clearly demonstrated in Fig. 5, where the grid that was used for the 23-deg angle case and the surface pressure along the centerline are shown. The calculated pressure agrees well with the experimental pressure away from the outflow plane, whereas close to the outflow plane a divergence of the results is observed.

The Reynolds-averaged Navier–Stokes equations with the x derivative (streamwise direction) of the viscous terms ignored are solved at the grid points of the mesh. A second-order central difference is applied to the implicitly treated viscous fluxes. The inviscid fluxes are determined by an upwind total-variation-diminishing scheme, which uses Roe's approximate Riemann solver. Alternating Gauss–Seidel relaxation in the streamwise direction is employed.

Because of the simplicity of the configuration geometry, the mesh was generated algebraically. Clustering was applied close to the plate and to the fin for adequate resolution of the viscous effects. For both configurations, at each crossflow plane 91 × 101 points (z, y directions) are used. In the streamwise x direction there are 117 grid planes uniformly spaced for the 23 × 23 deg test case (long fins) and 127 grid planes for the 18 × 18 deg test case (short fins). The inflow plane is located at a distance equal to $2\delta_0$ upstream of the leading edge of the fin. The height of the computational field is $26.8\delta_0$. For the simulation of the undisturbed boundary layer, 45 points are used. A constant spacing of $\Delta x = 0.5\delta_0$ was used in the x direction. The first point off the surface had a distance from the plate $\Delta y = 0.0006\delta_0$ and from the fins $\Delta z = 0.026\delta_0$. In the incoming boundary layer, the value of y^+ for the first grid point above the surface was $y^+ = 0.15$. An effort to decrease the Δz spacing was not successful because of numerical instability. The fact that

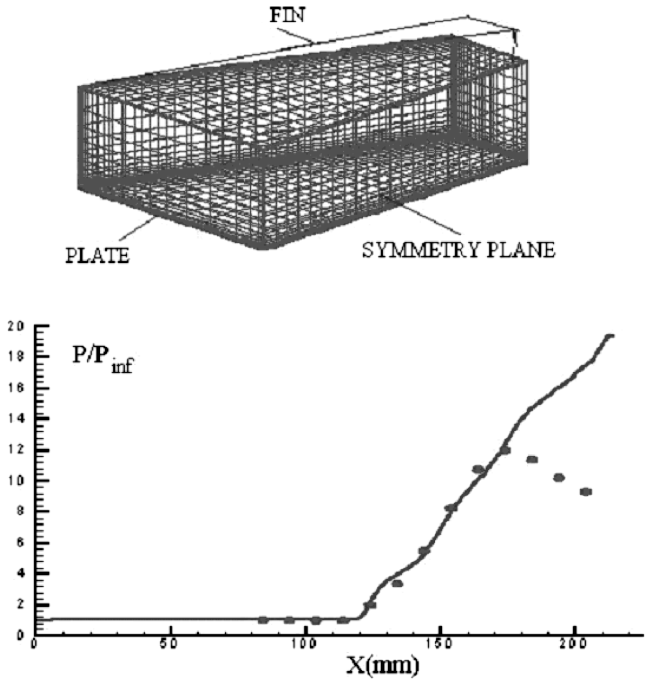

Fig. 5 Grid used for 23 × 23 deg configuration and pressure distribution along the symmetry line.

the grid is not very fine close to the fins can have an adverse effect on the predicted flow in the central part of the uniform area duct of the 18 × 18 deg test case.

The walls are assumed impermeable, and no-slip boundary conditions are applied. The boundary-layer profile upstream of the interaction region is used as boundary condition on the inflow plane and as initial condition for the whole flowfield. This profile was calculated by a two-dimensional procedure, from the leading edge of the flat plate to the edge of the fin. The symmetry condition was applied along the centerline of the plane. (The velocity component that is normal to the symmetry plane is assumed equal to zero.) The gradients of the flow parameters are set equal to zero on the upper and outflow far-field boundaries. The pressure gradient normal to the walls is taken to be zero. The temperature of the walls is assumed constant (isothermal condition) with $T_{\text{wall}}/T_{\text{adiabatic}} = 4.15$.

The required reference point for the calculation of the wake function within the separation domain [Eq. (6)] was selected as follows. Between the inflow plane and the region of confluence of the separation vortices, the centerline point (attached flow) was selected as the reference point at each streamwise station. Because downstream of the confluence the whole flow is separated, the reference point was fixed on the centerline upstream of the separation.

2. Comparison with the Experiments

The 23 × 23 deg experimental oil-flow visualization is compared with the computed skin-friction line patterns in Fig. 6. It is observed in Fig. 6 that the computations accurately reproduce the topological features shown in the experiment. Superposition of the results has shown that the separation lines coincide, whereas the computed secondary separation lines are very close to the experimental ones. A small quantitative difference is observed at the end of the surface imprint of the interacting separation vortices, where, as we have already mentioned, the simulation is not very accurate.

Schuelein and Zheltovodov[8] have measured the wall pressure at numbered cross sections in Fig. 6. The experimental and the computed crossflow wall-pressure distributions are compared in Fig. 7 for the 23 × 23 deg test case. The origin of the z axis corresponds to the centerline of the configuration. It is seen in this figure that the results that are based on the new eddy-viscosity model agree very well with the experimental evidence. In most of the stations, the predictions and the experimental data coincide. A small disagreement is observed in the region close to the centerline at station $x = 124$ mm, just downstream of the intersection of the primary separation lines. The small isle, which is generated there (see Fig. 6), is difficult to simulate quantitatively. In our opinion, the difficulty is caused by the fact that the flow in the isle is fully turbulent because it is fed by the upstream attached boundary layer. On the contrary, the applied turbulence model considers it as quasi-laminar.

The agreement of the calculated skin-friction lines with the experimental evidence is also good in the case of the short-fins configuration (angles: 18 × 18 deg), shown in Fig. 8. In this case the experiments did not reveal the existence of a secondary separation. The calculations also do not indicate such a feature. A small disagreement is observed in the spanwise extent of the central structure; in the calculations it has a smaller width.

The comparison of the wall pressure is shown in Fig. 9 for the short-fins configuration. Again, there is good agreement of the computed pressure distributions with the experimental pressures at the various cross sections. Small differences are observed mostly

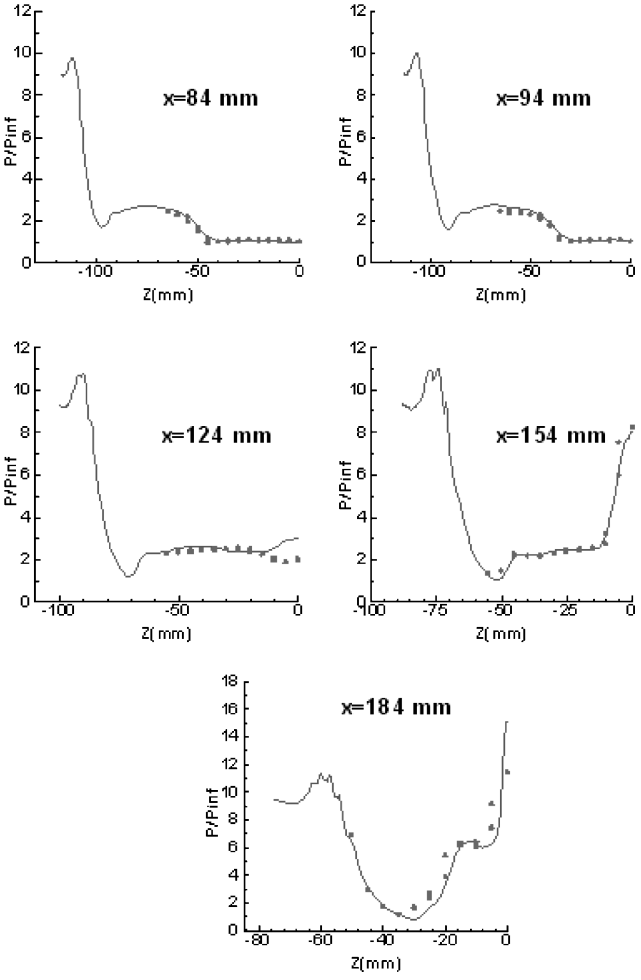

Fig. 7 Comparison of surface pressure. Crossing shocks: $M = 5.0$ and $\beta = 23$ deg.

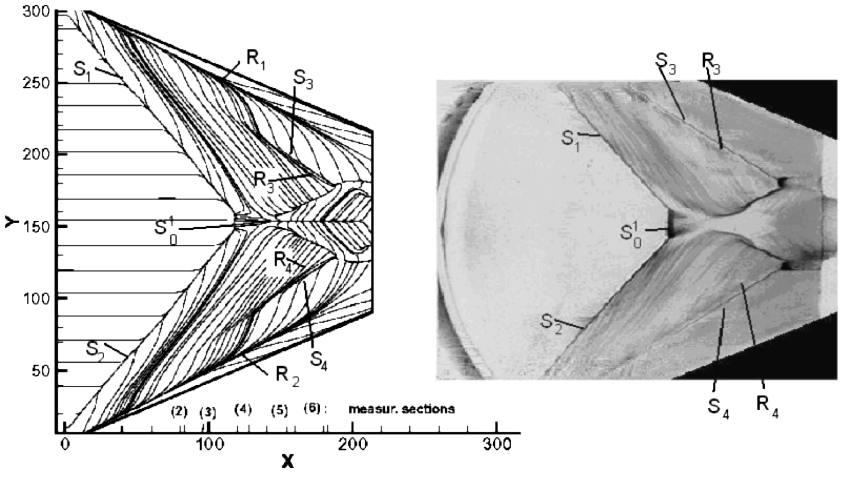

Fig. 6 Comparison of calculated skin-friction lines with oil-flow experiments: 23 × 23 deg configuration.

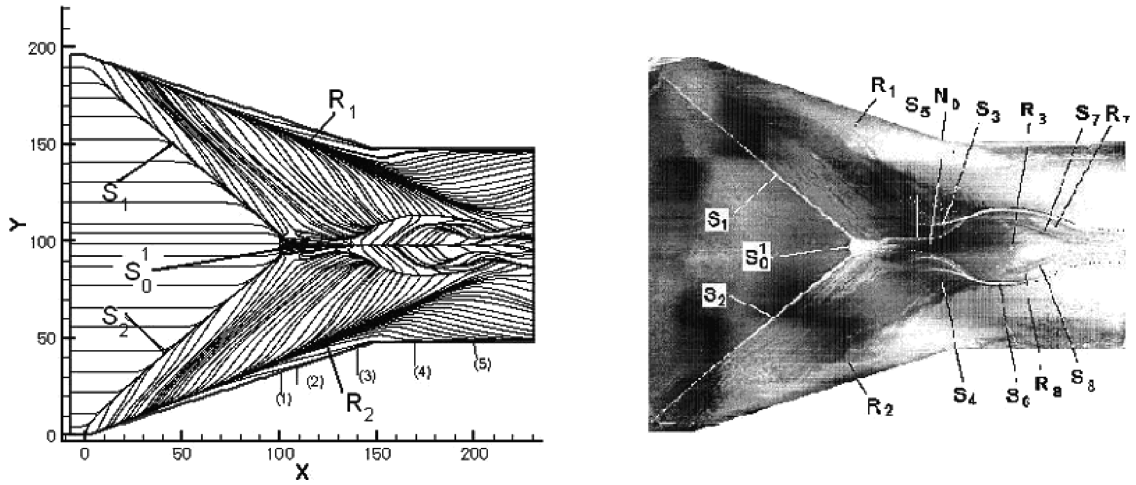

Fig. 8 Comparison of calculated skin-friction lines with oil-flow experiments: 18 × 18 deg configuration.

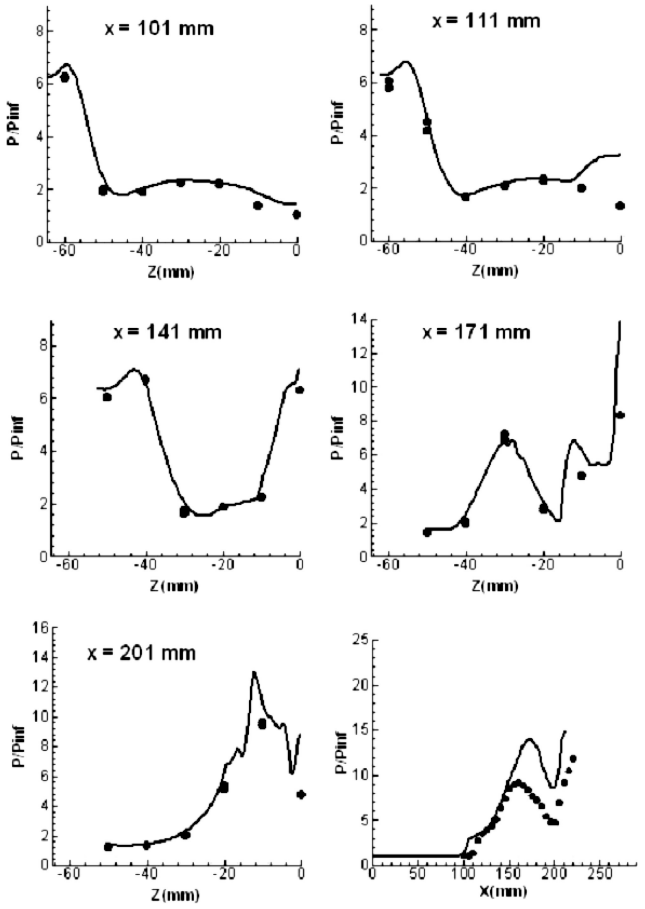

Fig. 9 Comparison of surface pressure. Crossing-shocks: $M = 5.0$ and $\beta = 18$ deg.

close to the centerline. Close to the fin there is better agreement. In this configuration also, the small isle downstream of the intersection of the primary separation lines is not simulated perfectly (station $x = 111$ mm; Fig. 9). The predicted centerline pressure at the downstream part of the constant cross-section duct (between $x = 160$–210 mm) is very bad. This region is quite upstream of the outflow plane, so that the cause of the disagreement is not the incorrect simulation of the outflow conditions. Possibly the bad agreement reflects the incorrect simulation of the mutual interaction of the crossing shocks and the effect of the rarefaction waves on them.

B. High-Angle-of-Attack Calculations

The high-angle-of-attack test cases were calculated using an implicit, approximately factored, partially flux-split algorithm, based on the thin-layer equations. The same code was used by Panaras and Steger[10] for the calculation of the flow about a prolate spheroid, using an ad hoc modification of the Baldwin–Lomax turbulence model. The grid was generated by solving a system of hyperbolic differential equations; a two-dimensional grid was generated in the symmetry plane, and then the three-dimensional grid was obtained by rotating it about the streamwise axis. Because there is no yaw angle, a symmetry plane calculation was applied to all computed flows.

1. *Supersonic Ogive Cylinder*

An experimental study of the flow around a three-caliber tangent ogive-cylinder body in a supersonic flow was conducted at ONERA with the aim of constituting an experimental database for code validations.[11] Results were obtained for a laminar boundary layer on the body and for transition tripped at $x/D = 1.0$. The test conditions were $M = 2$, $Re_L = 1.44 \times 10^6$, and incidence $\alpha = 10$–20 deg. The measurements include surface-pressure distributions at various cross sections. Side and cross views of the body are shown in Fig. 10, where the calculated shock waves and the crossflow vortices are shown for the turbulent $\alpha = 20$ deg flow. The half-body grid consists of 67 points in the streamwise direction, 71 in the circumferential, and 85 outward from the surface of the ogive-cylinder. The range of y^+ on the first layer of points above the surface of the body was $y^+ = 0.4$–1.0.

In the calculations, laminar flow was assumed from the tip of the body to the station $x/D = 1.0$. Downstream of this point, the turbulence model described in Sec. II.B was applied. For the $\alpha = 10$ deg test case, the calculated wall-pressure distribution along the circumferential direction θ is compared with the experimental data at four axial stations in Fig. 11. The agreement is good, especially at the downstream stations where the secondary separation is reproduced by the calculations. The small disagreement that is observed at the station $x/D = 4.95$ might indicate that the flow there is not completely turbulent but transitional.

The $\alpha = 20$ deg results are shown in Fig. 12. Two sets of calculation are included in this figure. Calc. 1 (dashed lines) denotes the turbulent-flow results. In this case the agreement of the calculations with the experiments is very good, except near $\theta = 80$ deg, where the flow separates. The suction there is overestimated in the calculations. This small disagreement was not expected because the quality of the results is high at the fully separated flow on the leeward side of the body (perfect reproduction of the plateau pressure). For this reason we repeated the calculations employing the same turbulence model but with the value of the constant α of Eq. (4b) reduced to $\frac{1}{8}$ of the regular $\alpha = 3.0$ value. The results obtained are those denoted with the solid line (calc. 2). An improvement in the results

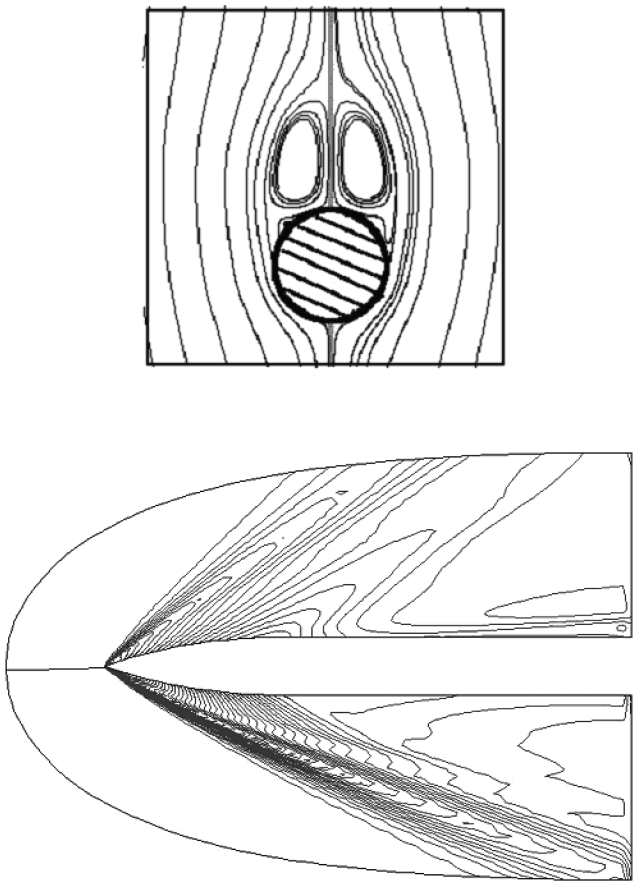

Fig. 10 Ogive-cylinder flow: $M = 2.0$ and $\alpha = 20$ deg (calculated results).

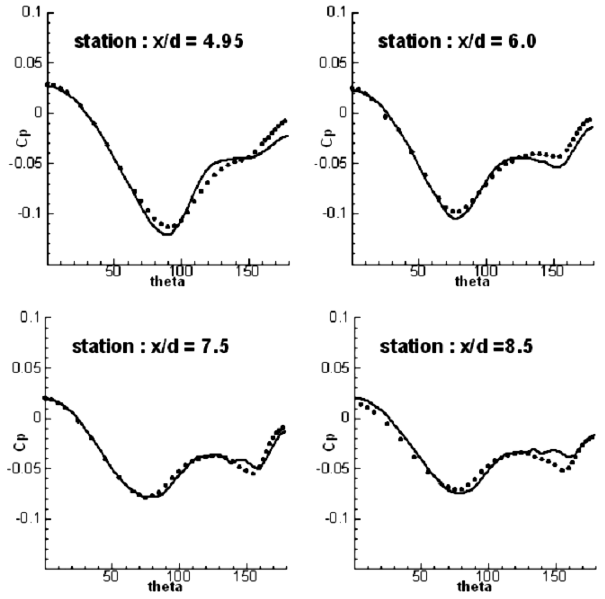

Fig. 11 Ogive-cylinder flow at $\alpha = 10$ deg: surface-pressure comparison.

is observed. The suction values near $\theta = 80$ deg are almost equal to those found experimentally. In the other locations the two sets of calculation coincide completely. This behavior indicates, in our opinion, that most probably the experimental artificial trip of transition is not very effective as the flow angle is increased.

2. Subsonic Prolate Spheroid

The prolate spheroid is a body of simple geometry that can provide significant understanding of the complex flow that can develop

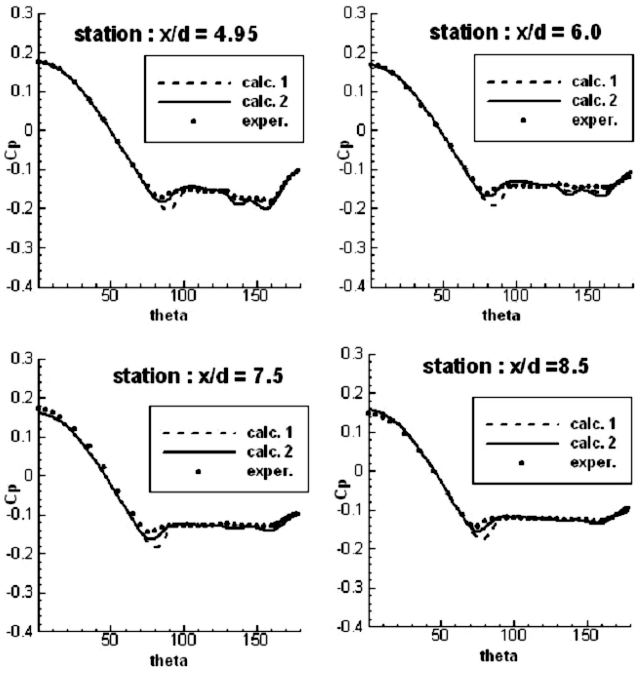

Fig. 12 Ogive-cylinder flow at $\alpha = 20$ deg: surface-pressure comparison.

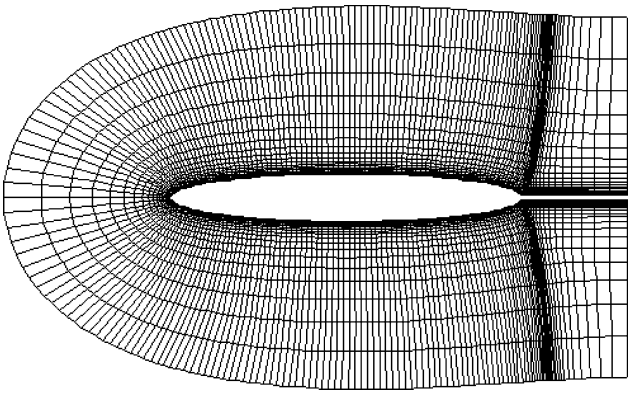

Fig. 13 Grid about the 6:1 prolate spheroid.

about slender bodies at incidence. A variety of wind-tunnel tests have been carried out for a 6:1 prolate spheroid at DLR, at Goettingen, using a glass-fiber model of 4-mm wall thickness and having major and minor axis of 2.4 and 0.4 m, respectively. The majority of the tests have been carried out at moderate Reynolds numbers, but some measurements have also been conducted in collaboration with ONERA, in France, at higher Reynolds numbers. The tests have been used by an AGARD Working Group[12] for assessing the capability of boundary-layer solvers. In the present study, only the ONERA tests have been simulated. The test conditions are $\alpha = 30$ deg, $U = 75$ m/s, and $Re_L = 43 \times 10^6$. In the present calculations, the half-body grid consists of 121 points in the streamwise direction, 51 in the circumferential, and 65 outward from the surface of the ogive-cylinder. The flow parameter y^+ at the first layer of points above the surface was $y^+ = 0.8$–1.5. A part of the sting that supported the prolate spheroid in the wind tunnel is included in the calculations (Fig. 13).

The computed and the experimental pressure coefficients are compared along the circumferential direction φ in Fig. 14, at three axial locations. The agreement is very good, not only on the windward but also on the leeward side. The perfect simulation of the plateau pressure across the separated part of the flow at the location $x/L = 0.81$ is remarkable. (L is the length of the major axis.) The suction observed at $\varphi = 160$ deg at the $x/L = 0.53$ and 0.81 locations is caused by the existence of secondary separation.

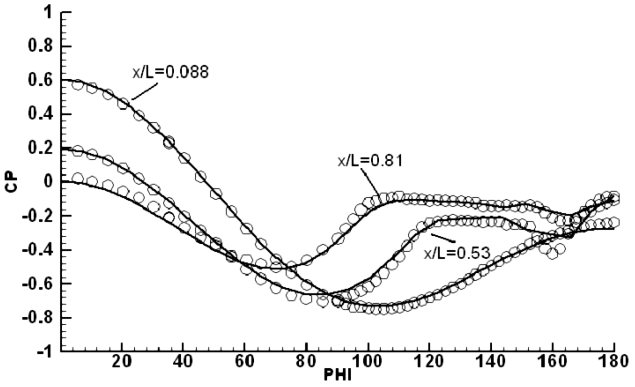

Fig. 14 Prolate spheroid flow at $\alpha = 30$ deg: surface pressure.

IV. Conclusions

This work is an extension of application of the modified by the present author[3] algebraic turbulence model of Baldwin–Lomax to other types of flows than single-fin/plate supersonic swept-shock-wave/turbulent-boundary-layer interactions. It has been demonstrated that supersonic or subsonic high-angle-of-attack flows can be simulated confidently if the eddy-viscosity relations derived in Ref. 3 are applied. Details are given regarding the selection of the required reference point for the determination of the wake function.

In the case of strong crossing-shocks/turbulent-boundary-layer interactions, the standard modified model gave very bad results in the region of interaction of the two flat vortices, which are generated by the individual fins. However, a generalization of the basic equation of the modified model aimed at increasing the eddy viscosity in the region of interaction of the two separation vortices improved the results.

Actually, Eqs. (4b) and (6) can be considered as subcases of the general formula

$$F_{\text{wake}} = \frac{\alpha(\eta_{\text{ref}} F_{\text{ref}})^{q+1}}{(\eta_{\max} F_{\max})^{q}} \tag{7}$$

where for single-fin/plate interactions or high-incidence flows $q = 1$, and for the more complicated crossing-shocks interactions $q = \frac{1}{2}$.

Experience has shown that reliable results are obtained when the value of the constant α is in the range $\alpha = 3.0$–5.0. For the calculated single-fin and high-incidence test cases, the value $\alpha = 3.0$ provided the best results. For the crossing shocks, the agreement was better with $\alpha = 4.0$. However, any value of α within the aforementioned range gives acceptable results.

References

[1]Panaras, A. G., "The Effect of the Structure of Swept Shock-Wave/Turbulent Boundary-Layer Interactions on Turbulence Modeling," *Journal of Fluid Mechanics*, Vol. 338, 1997, pp. 203–230.

[2]Settles, G. S., and Dodson, L. J., "Hypersonic Shock/Boundary-Layer Interaction Database," NASA CR-177577, April 1991.

[3]Panaras, A. G., "Algebraic Turbulence Modeling for Swept Shock-Wave/Turbulent Boundary-Layer Interactions," *AIAA Journal*, Vol. 35, No. 3, 1997, pp. 456–463.

[4]Knight, D. D., and Degrez, G., "Shock Waves Boundary Layer Interactions in High Mach Number Flows. A Critical Survey of Current Numerical Prediction Capabilities," AGARD-AR-319, Vol. 2, Dec. 1998, pp. 1.1–1.35.

[5]Baldwin, B. S., and Lomax, H., "Thin Layer Approximation and Algebraic Model for Separated Turbulent Flows," AIAA Paper 78-257, Jan. 1978.

[6]Hung, C. M., and MacCormack, R. W., "Numerical Solution of Three-Dimensional Shock Wave and Turbulent Boundary-Layer Interaction," *AIAA Journal*, Vol. 16, No. 10, 1978, pp. 1090–1096.

[7]Knight, D. D., "Numerical Simulation of 3-D Shock Wave Turbulent Boundary Layer Interaction," AGARD-R-792, Paper 3, Aug. 1993.

[8]Schuelein, E., and Zheltovodov, A. A., "Development of Experimental Methods for the Hypersonic Flows Studies in Ludwieg Tube," *International Conference on the Methods of Aerophysics Research: Proceedings Part I*, 1998, pp. 191–199.

[9]Schmisseur, J. D., and Gaitonde, D. V., "Numerical Investigation of New Topologies in Strong Crossing Shock Wave/Turbulent Boundary Layer Interactions," AIAA Paper 2000-0931, Jan. 2000.

[10]Panaras, A. G., and Steger, J. L., "A Thin-Layer Navier–Stokes Solution of the Flow About a Prolate Spheroid," *Zeitschrift fuer Flugwissenschaften und Weltraumforschung*, Vol. 12, No. 3, 1988, pp. 173–180.

[11]Barberis, D., "Supersonic Vortex Flow Around a Missile Body," AGARD AR-303, Vol. 2, Aug. 1994.

[12]"Calculation of 3D Separate Turbulent Flows in Boundary Layer Limit," AGARD, AR-255, May 1990.

R. So
Associate Editor